alpha-adrenergic (*9*) or beta-adrenergic (*10*) receptors. In addition, the microvessel preparations used here were more than 95 percent pure as determined by light (including phase-contrast) microscopy and transmission and scanning electron microscopy (*6*). These considerations, along with the negligible levels of serotonin, benzodiazepine, opiate, and muscarinic cholinergic receptors, strengthen the conclusion that the adrenergic and histamine 1 receptors involve cerebral microvessels. Despite the relative microvessel enrichment of histamine 1 and adrenergic receptors, microvessels, which account for < 1 percent of the brain's mass, provide only a small portion of the brain's total content of these receptors.

In general, alpha agonists constrict and beta agonists dilate cerebral vessels (*1*), whereas serotonin constricts or dilates depending on the route of administration, species, and state of vascular contractility (*11*). The negligible serotonin receptor binding detected here [despite apparent serotonin innervation of cerebral microvessels (*6*)] may reflect species or regional variation. Histamine, localized in mast cells surrounding cerebral blood vessels (*12*), may account for histamine-elicited constriction as well as dilatation via a histamine 2 receptor-linked adenylate cyclase (*13*).

The existence of norepinephrine and histamine receptors in the brain's microvessels suggests that these transmitters are endogenous regulators of the microcirculation. Drugs that affect these receptor sites might be useful in treating cerebral blood vessel abnormalities.

STEPHEN J. PEROUTKA
Departments of Pharmacology and Experimental Therapeutics and *Psychiatry and Behavioral Sciences, Johns Hopkins University School of Medicine, Baltimore, Maryland 21205*
MICHAEL A. MOSKOWITZ
Laboratory of Neuroendocrine Regulation, Department of Nutrition and Food Science, Massachusetts Institute of Technology, Cambridge and *Section of Neurology, Peter Bent Brigham Hospital, Harvard Medical School, Boston, Massachusetts 02115*
JOHN F. REINHARD, JR.
Laboratory of Neuroendocrine Regulation, Massachusetts Institute of Technology
SOLOMON H. SNYDER
Departments of Pharmacology and Experimental Therapeutics and *Psychiatry and Behavioral Sciences, Johns Hopkins University School of Medicine*

References and Notes

1. W. Kuschinsky and M. Wahl, *Physiol. Rev.* **28**, 656 (1978).
2. M. E. Raichle, B. K. Hartman, J. O. Eichling, L. G. Sharpe, *Proc. Natl. Acad. Sci. U.S.A.* **72**, 3726 (1975).
3. T. Donath, *Acta Morphol. Acad. Sci. Hung.* **16**, 285 (1968); B. K. Hartman, D. Zide, S. Udenfriend, *Proc. Natl. Acad. Sci. U.S.A.* **69**, 2722 (1972); M. L. Rennels and E. Nelson, *Am. J. Anat.* **144**, 233 (1975).
4. F. M. Lai, S. Udenfriend, S. Spector, *Proc. Natl. Acad. Sci. U.S.A.* **72**, 4622 (1975).
5. T. J. Herbst, M. E. Raichle, J. A. Ferrendelli, *Science* **204**, 330 (1979); J. Nathanson and G. Glaser, *Nature (London)* **278**, 567 (1979).
6. J. F. Reinhard, Jr., J. E. Liebmann, A. J. Schlosberg, M. A. Moskowitz, *Science* **206**, 85 (1979).
7. L. I. Larrson, L. Edvinsson, J. Fahrenkrug, R. Hakanson, C. Owman, O. Schattalitzky, D. Muckadell, F. Sundler, *Brain Res.* **113**, 400 (1976); V. Chan-Palay, *Wenner-Gren Cent. Int. Symp. Ser.* **30**, 39 (1977); *Brain Res.* **102**, 103 (1976).
8. B. Mrsulja, B. J. Mrsulja, T. Fujimoto, I. Klatzo, M. Spatz, *Brain Res.* **110**, 644 (1976).
9. D. C. U'Prichard, D. A. Greenberg, S. H. Snyder, *Mol. Pharmacol.* **13**, 454 (1977).
10. J. R. Sporn, B. B. Wolfe, T. K. Harden, P. B. Molinoff, *ibid.* **13**, 1170 (1977).
11. L. Edvinsson, J. Cervosna, L. I. Larrson, C. Owman, A. L. Ronnberg, *Neurology* **27**, 878 (1977); L. Edvinsson and J. E. Hardebo, *Acta Physiol. Scand.* **97**, 523 (1976).
12. B. Jarrott, J. T. Hjelle, S. Spector, *Brain Res.* **168**, 323 (1979).
13. L. Edvinsson and C. Owman, *Neurology* **25**, 271 (1975).
14. J. P. Bennett, Jr., in *Neurotransmitter Receptor Binding*, H. I. Yamamura, S. J. Enna, J. J. Kuhar, Eds. (Raven, New York, 1978), pp. 57-90.
15. S.J.P. is a recipient of medical scientist training program grant 5T 32 GM0309 from NIH. M.A.M. is an established investigator of the American Heart Association. This work was supported by PHS grants HL-22573-01, NS-15201 (M.A.M.), MH-18501, DA-00266 (S.H.S.), and by grants from the McKnight and Hartford foundations. The authors thank R. M. Lebovitz for excellent technical assistance and D. C. Hanks for manuscript preparation.

26 December 1979; revised 11 February 1980

Single-Shot Channel Activation Accounts for Duration of Inhibitory Postsynaptic Potentials in a Central Neuron

Abstract. *In the goldfish Mauthner cell, inhibitory postsynaptic currents evoked by intracellular stimulation of presynaptic neurons decay exponentially, with a mean time constant of 6.65 milliseconds. Analysis of membrane conductance fluctuations induced by iontophoresis of glycine and γ-aminobutyric acid indicates a mean inhibitory channel lifetime of 7.15 milliseconds. The results thus suggest that the relaxation kinetics of activated inhibitory channels are rate-limiting during decay of the inhibitory postsynaptic current.*

Inhibitory postsynaptic potentials (IPSP's) recorded from vertebrate central neurons, particularly those in the brain, are often long lasting (*1*), presumably because of (i) a prolonged elevation of inhibitory transmitter concentration in the synaptic cleft or (ii) a long mean lifetime of activated inhibitory channels. The first possibility implies that repetitive transmitter-receptor interactions, resulting perhaps from repetitive firing of the presynaptic terminals, restricted diffusion of the transmitter from the synaptic cleft, or relatively slow transmitter uptake, contribute to the underlying inhibitory postsynaptic current (IPSC). In contrast, the second possibility implies that transmitter concentration falls rapidly at active synapses, with IPSC duration reflecting the relaxation kinetics of inhibitory channels, most of which open only once. In the case of the frog neuromuscular junction, Magleby and Stevens (*2*) and Anderson and Stevens (*3*) concluded that channel gating properties, rather than the loss of acetylcholine from the endplate region, are rate-limiting during the normal endplate current decay. That conclusion was based in part on results obtained with the analysis of conductance fluctuations (*4*). This analytical approach, however, has been restricted so far to peripheral junctions (*3, 4*) and to neurons in vitro (*5*); it has not yet been applied to vertebrate central neurons in situ, where the experimental analysis is more difficult.

Having analyzed inhibition at the goldfish Mauthner cell (M-cell) (*6, 7*), we now present evidence, based on measurements of both unitary IPSC decay and conductance fluctuations, that suggests that most channels open and close only once during an IPSP. Our results thus extend to at least some central neurons the basic findings of Stevens and his colleagues.

Goldfish (*Carassius auratus*) 12 to 18 cm long and immobilized with curare (0.15 mg) were used. The procedures for artificial respiration, exposure of the medulla, and identification of the M-cell after its antidromic activation, were similar to those described previously (*8-10*). Intracellular recordings were obtained from the M-cell soma or proximal lateral dendrite. Injections of Cl^- ion from the intracellular recording electrodes were used to displace the IPSP reversal potential (*11*) so the recorded IPSP's were depolarizing. In the first of these experimental series, we obtained intracellular recordings simultaneously from identified interneurons (Fig. 1A), the so-called passive hyperpolarizing potential (PHP) cells (*10*), which have been shown to me-

0036-8075/80/0509-0612$00.50/0

diate both electrical and chemical inhibitions of the M-cell (*6*); they were directly activated by transmembrane current pulses, and the transynaptically evoked M-cell responses were averaged on a signal averager (Nicolet 1074). This direct activation of single presynaptic neurons (*6, 7*) eliminates complications normally attributable to their repetitive firing, as during recurrent collateral inhibition of the M-cell (*6, 7, 9*). Finally, cross talk between the electrodes was reduced by painting the presynaptic electrode with conducting silver paint and connecting this shield to ground.

Figure 1B illustrates a typical monosynaptic unitary IPSP recorded from the M-cell after a presynaptic impulse. This IPSP lasts approximately 15 msec, which is more than one order of magnitude longer than the M-cell time constant of 0.2 to 0.4 msec (*8, 12*). It follows that unitary IPSP decay should be a direct measure of the underlying conductance increase, that is, of postsynaptic current. This conclusion was confirmed by pairing unitary IPSP's with the M-cell's antidromic impulse, which is passively conducted in the cell's soma and lateral dendrite (*8, 13*). Consequently, any reduction in spike height is proportional to the membrane conductance increase; the decays of both parameters have indeed the same time course (Fig. 1C).

To analyze the factors determining IPSC duration, we first measured the decay phases of computer-averaged unitary IPSP's (Fig. 2A). If IPSC decay is rate-limited by the closure of activated inhibitory channels, it should be exponential with a time constant, τ_{IPSC}, equal to the mean channel lifetime, τ_c (*2, 3*). Semilogarithmic plots (Fig. 2B) of unitary IPSP decay phases ($N = 46$) closely fit straight lines (linear regression analyses, P always $< .001$). The mean τ_{IPSC} was 6.63 msec, with a range of 3.5 to 11.9 msec (standard deviation = $\pm$ 2.13 msec). The histogram of this distribution (Fig. 2C) appears unimodal, and there is no present explanation for the wide range of time constants. For example, there was no correlation between τ_{IPSC} and either the magnitude of individual unitary IPSP's or their quantal content, which ranged from 1.88 to 30.0.

The second experimental series employed iontophoretic applications of either γ-aminobutyric acid (GABA) (4*M*, *p*H 4.3), glycine (2*M*, *p*H 3.0), or glutamate (2*M*, *p*H 7.3 to 8.5). Extracellular recordings were used to position the drug-filled pipette within 25 μm of the recording pipette and in the region giving the maximum drug-induced depolarization. (This location was typically as close to the M-cell membrane as possible.) The results were obtained after topical application of 100 m*M* $MgSO_4$. This procedure was necessary to (i) reduce background synaptic noise and (ii) prevent presynaptic drug effects on transmitter release. Although Mg^{2+} did reduce background noise by at least a factor of 2 and did block auditory-evoked M-cell responses, the observations obtained before and after its application were qualitatively the same. Membrane potential fluctuations were recorded and analyzed by standard techniques. During each trial the power spectra of five to ten half-second segments were averaged before and during the late phase, or tail, of the drug effect, and the difference spectra were then computed.

Glycine and GABA were chosen because they increase M-cell Cl^- conductance (*2, 14*), with the former being the most likely candidate for the inhibitory transmitter acting on this neuron. Iontophoretic application of either drug

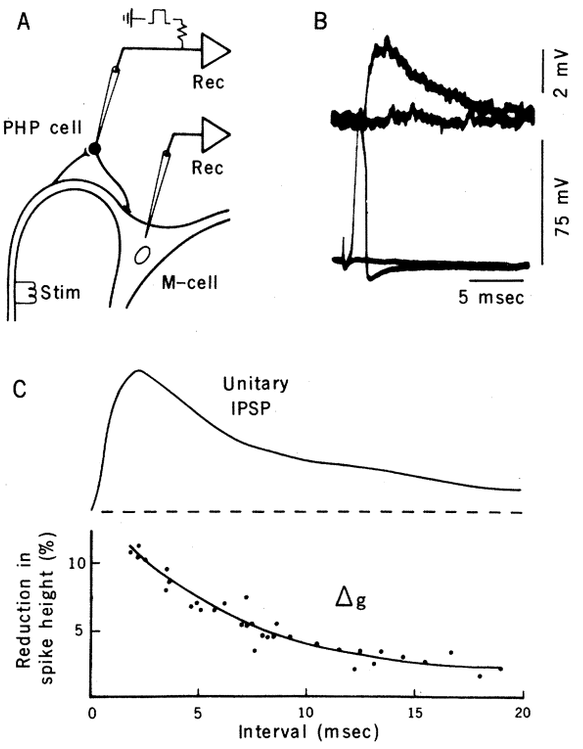

Fig. 1. Properties of unitary IPSP's recorded in the Mauthner (*M*) cell after single presynaptic impulses. (A) Experimental arrangement used for simultaneous intracellular recordings (*Rec*) from and stimulation of both the *M-cell* and a presynaptic inhibitory interneuron (*PHP cell*) belonging to the recurrent collateral network, both neurons having been identified by their characteristic responses to antidromic stimulation of the M-axon in the spinal cord (*Stim*). (B) Typical unitary monosynaptic depolarizing IPSP recorded in an M-cell injected with Cl^- (upper trace) after a single presynaptic impulse (lower trace). Stimulus current (not illustrated) straddled the threshold for spike initiation in the two superimposed traces. (C) Comparison of the IPSP decay (upper tracing) and of the underlying conductance change (Δg), the latter evaluated from the reduction in the amplitude of a test antidromic spike elicited at the indicated intervals after IPSP onset. Each data point is a computed average of at least five successive measurements and is expressed as the percentage of reduction relative to control spike height. The decay phases of the IPSP and of the conductance increase are parallel. [Data illustrated in (B) and (C) are from two different experiments.]

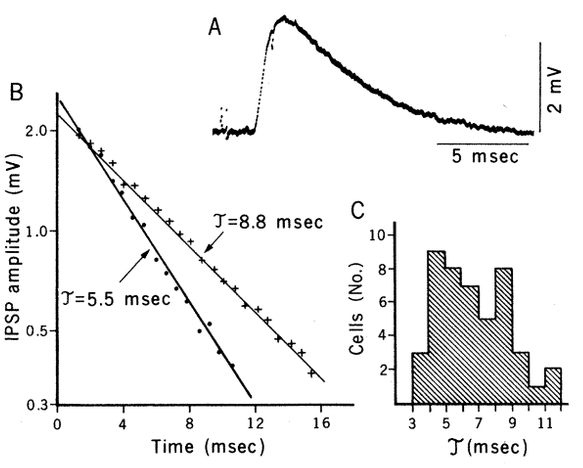

Fig. 2. Exponential decay of unitary inhibitory postsynaptic current, determined from IPSP measurements. (A) Typical computer-averaged IPSP ($N = 32$) used for time course analysis; decay was exponential, with $\tau = 5.0$ msec when determined in a manner similar to that illustrated in (B). (B) Semilogarithmic plots of IPSP amplitude versus time and calculated linear regression lines for two other cells. Both relationships are linear, yielding respective time constants of 8.8 msec ($\log_{10} V = 0.36 - 0.049t$; where V is voltage and t is time; $r^2 = .999$; $P < .001$) and 5.5 msec ($\log_{10} V = 0.4 - 0.78t$; $r^2 = .992$; $P < .001$). (C) Histogram of IPSP decay time constants for 46 different responses obtained in 24 experiments.

for periods as long as 1 second typically produced a large increase in M-cell conductance, which peaked within a few seconds and gradually decayed during the next 10 to 20 seconds (Fig. 3A for GABA). The records in Fig. 3B, which are from the same experiment, illustrate that this conductance change was associated with a drug-induced depolarization of comparable time course; similarly, the membrane noise initially decreased and then increased above the control level during the tail of the drug-induced depolarization. This sequence is readily explained: during the peak depolarization, (i) the background noise will be shunted by the high membrane conductance, and (ii) the noise from the activated inhibitory channels will be minimal since the membrane potential will be close to the Cl^- equilibrium potential. During the later phase of the response, the shunt effect is less and the driving force for Cl^- ion movement becomes greater.

The enhanced noise (Fig. 3B) is the most dramatic example observed. In other instances, increased activity was either just detectable (Fig. 3C, from a glycine experiment) or could not be readily discerned visually. Nevertheless, computer analysis indicated a consistent increase in total signal power during the tail of the drug effects.

The power spectral densities of GABA- and glycine-induced membrane potential fluctuations were calculated during this late phase of the drug effect. In 20 experiments, the difference spectra could be approximated by a single Lorentzian of the form $S(f) = A/[1 + (f/f_c)^2]$, where $S(f)$ is the difference spectrum as a function of frequency, f, and f_c is the frequency at which the power has decreased to half its asymptotic value, A. Examples of these results for the GABA and glycine experiments of Fig. 3, B and C, are shown in Fig. 3, D and E, respectively. The approximation of the data by a single Lorentzian is consistent with the hypothesis that the fluctuations arise from a single population of activated channels whose lifetime is exponentially distributed, with the average lifetime, τ_c, being equal to $1/2\pi f_c$ (*3*). The average value of τ_c was 7.15 msec (range, 4.5 to 10.6 msec), with no significant difference between the results obtained with glycine or GABA. This mean value is in close agreement with that obtained from the measurements of unitary IPSP decay; it suggests that IPSP duration can reasonably be attributed to the relaxation kinetics of a population of inhibitory channels activated only once.

The interpretation of our results depends on the fact that the two independent experimental approaches yield effectively the same time constants, particularly since noise analysis in a central vertebrate neuron is difficult. Given the experimental complications and possible errors resulting from conductance effects on background noise, the Lorentzian fits appear reasonable, as does the agreement between τ_c and τ_{IPSC}. Also, in four experiments with glutamate iontophoresis, the calculated spectra had a significantly higher cutoff frequency, indicating a mean channel lifetime in the range of 2 to 4 msec. This observation provides an internal check on the noise analysis technique and is consistent with observations that excitatory postsynaptic potential duration in the M-cell is significantly (two to three times) shorter than that of IPSP's recorded in the same cell.

From our results, we can infer that inhibitory transmitter concentration must decay rapidly after its release. Since glycine is the putative transmitter and since there is no specific mechanism for inactivating this amino acid (such as exists at the vertebrate neuromuscular junction for acetylcholine), it would be of interest to determine whether diffusion alone or a specific high affinity glycine uptake (*15*) could act so rapidly.

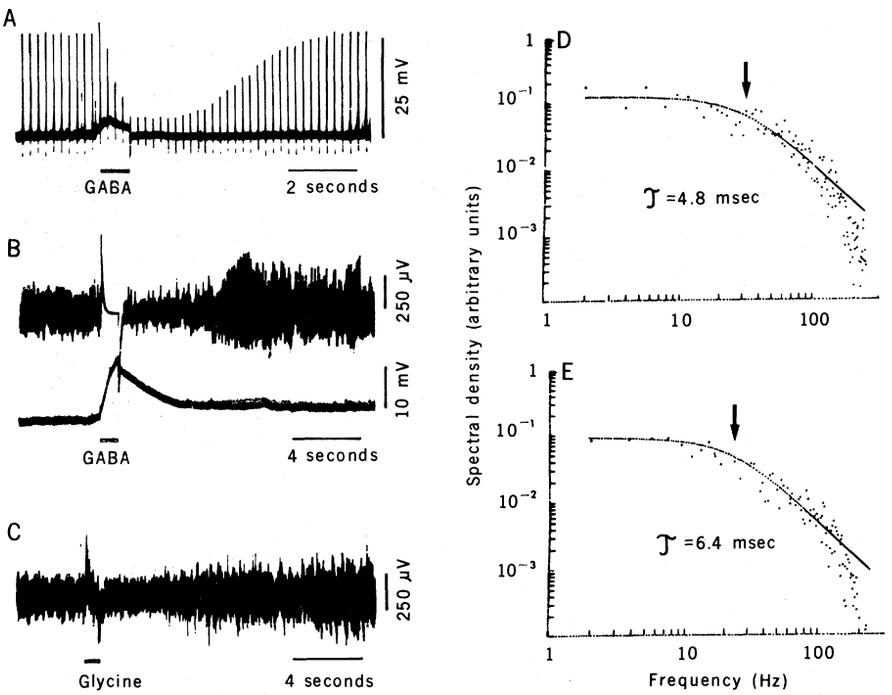

Fig. 3. Conductance changes and potential fluctuations of the M-cell induced by iontophoretic applications of GABA and glycine. All data were obtained from preparations treated with Mg^{2+}; the intracellular recordings were from the soma or proximal lateral dendrite of M-cells injected with Cl^-. (A and B) Responses evoked by GABA. (A) Prolonged conductance change after drug application, indicated by the reduction in antidromic spike height (a-c coupled recording). (B) Example of increased voltage fluctuations (upper trace) during the tail of a GABA-induced depolarization (lower trace). (C) Visible, but less dramatic, increased noise fluctuations attributable to glycine. (D and E) Power density spectra of amino acid–induced potential fluctuations obtained, respectively, during the trials illustrated in (B) and (C). The spectra shown are the averaged differences between those obtained before the drug application and during the late phase, or tail, of its effect. (D) The GABA data points fit a single Lorentzian curve with a cutoff frequency of 33 Hz (arrow), indicating a mean channel open-time, τ, of 4.8 msec. (E) The data obtained with glycine also fit a Lorentzian, with a half-power frequency of 25 Hz (arrow) and, therefore, a τ of 6.4 msec. In each plot the deviation from the fit at high frequencies is due to the six-pole low-pass filter (cutoff frequency = 200 Hz) used during the experiments.

DONALD S. FABER
HENRI KORN
Division of Neurobiology, Department of Physiology, State University of New York, Buffalo 14214 and
INSERM U3, C.H.U. Pitie-Salpetriere, 75634 Paris Cedex 13, France

References and Notes

1. Examples include thalamic relay neurons [D. P. Purpura and B. Cohen, *J. Neurophysiol.* **25**, 261 (1962); P. Andersen, J. C. Eccles, T. A. Sears, *J. Physiol. (London)* **174**, 370 (1964)] and hippocampal pyramidal cells [E. R. Kandel, W. A. Spencer, F. J. Brinley, *J. Neurophysiol.* **24**, 225 (1961)]. See also J. C. Eccles [*The Inhibitory Pathways of the Central Nervous System* (Thomas, Springfield, Ill., 1969)].
2. K. L. Magleby and C. F. Stevens, *J. Physiol. (London)* **223**, 151 (1973); *ibid.*, p. 173.
3. C. R. Anderson and C. F. Stevens, *ibid.* **235**, 655 (1973).
4. B. Katz and R. Miledi, *Nature (London)* **226**, 962 (1970).
5. P. Ascher, A. Marty, T. O. Neild, *J. Physiol. (London)* **278**, 177 (1978); J. C. Nicholls and B. G. Wallace, *ibid.* **281**, 171 (1978); R. N.

McBurney and J. L. Barker, *Nature (London)* **274**, 596 (1978).
6. H. Korn and D. S. Faber, *Science* **194**, 1166 (1976).
7. D. S. Faber and H. Korn, in *Neurobiology of the Mauthner Cell*, D. S. Faber and H. Korn, Eds. (Raven, New York, 1973), p. 47.
8. E. J. Furshpan and T. Furukawa, *J. Neurophysiol.* **25**, 732 (1962).
9. H. Korn and D. S. Faber, *ibid.* **38**, 452 (1973).
10. D. S. Faber and H. Korn, *Science* **179**, 577 (1973).
11. T. Furukawa and E. J. Furshpan, *J. Neurophysiol.* **26**, 140 (1963); Y. Asada, *Jpn. J. Physiol.* **13**, 583 (1963).
12. Y. Fukami, T. Furukawa, Y. Asada, *J. Gen. Physiol.* **48**, 581 (1965).
13. J. Diamond, *J. Physiol. (London)* **194**, 669 (1968).
14. ———, S. Roper, G. Yasargil, *ibid.* **232**, 87 (1973).
15. F. A. Henn, *J. Neurosci. Res.* **2**, 271 (1976); T. Hokfelt and Å. Ljungdahl, *Brain Res.* **32**, 189 (1971); G. A. R. Johnston and L. L. Iversen, *J. Neurochem.* **18**, 1951 (1971).
16. Supported in part by NIH grant NS 12132, INSERM grant CRL 78.5.006.6, and a Ralph Hochstetter Medical Research Advance Award to H.K. in honor of H. C. Buswell and B. H. Buswell. We thank R. Mowry for computer programming, J. R. Teilhac for preparing the figures, and J. Jordan for typing the manuscript.

19 December 1979

A Disparity Gradient Limit for Binocular Fusion

Abstract. *Ever since Panum, it has been commonly assumed that there is an absolute disparity limit for binocular fusion. It is now found that nearby objects modify this disparity limit. This result sheds new light on several enigmatic phenomena in stereopsis.*

It is generally assumed that a stereoscopically presented object will appear fused and single if its binocular disparity falls within Panum's fusional area (*1*). When the disparity exceeds this limit, the object will appear double. An object's disparity may be measured relative to the vergence angle of the eyes or relative to another object in the visual field, such as a fixation point. According to the traditional view, the magnitude of this disparity (or disparity difference) is the critical parameter for fusion.

We find, however, that the disparity gradient rather than the disparity magnitude is the limiting factor for fusion when two or more objects occur near one another in the visual field. The disparity gradient is defined between nearby objects as the difference in their disparities divided by their separation in visual angle. Fusion of at least one object fails when this gradient exceeds a critical value (approximately 1).

To illustrate an implication of the disparity gradient constraint, consider two objects that are moved toward one another in the visual field, while the distances of the objects from an observer are held constant. The disparity gradient between the objects will increase in inverse proportion to object separation and must eventually exceed the gradient limit for fusion. Thus, each object may appear single when the two are widely separated, but when their angular separation becomes sufficiently small, singleness of one or both will necessarily give way to diplopia. This is true even for objects with very small disparities well within Panum's fusional limit.

The minimal stereogram in which the disparity gradient may influence fusion is composed of just two dots. The important geometric parameters of the stereogram are the dot separations, R_ℓ, R_r, and orientations Θ_ℓ, Θ_r, in the left and right half-images (Fig. 1A). The binocular dot separation, R_b, and orientation, Θ_b, are defined by the midpoints between the half-images of each dot in the binocular view (Fig. 1B).

The binocular disparity difference of the stereogram is defined as the difference between the individual dot disparities.

$$d_b = d_1 - d_2 = R_r \cos \Theta_r - R_\ell \cos \Theta_\ell$$

The disparity gradient for these dots may be defined as their binocular disparity difference divided by the binocular dot separation, d_b/R_b. It should be noted that

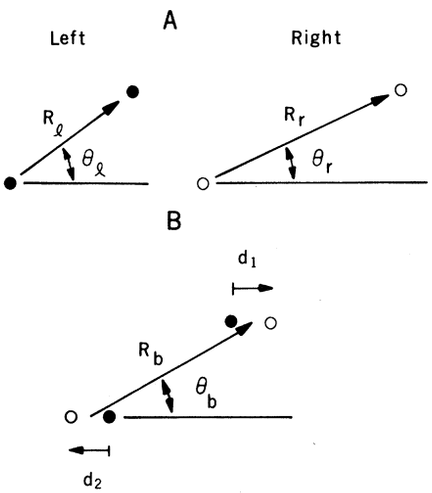

Fig. 1. Geometry of a two-dot stereogram. (A) The half images shown to each eye and (B) the physical pattern after binocular combination. There is no vertical disparity, so $R_\ell \sin \Theta_\ell = R_r \sin \Theta_r$. Dots seen by the left eye are shown as filled symbols and dots seen by the right eye as open symbols. In the stereograms these dots are identical.

R_b, Θ_b, d_b, and the disparity gradient depend only on stereogram geometry, and are independent of ocular vergence.

When the stereogram is binocularly combined (Fig. 1B), the upper and lower dots may appear at different depths, and their half images may appear fused (single) or diplopic (double). Diplopia occurs when disparities d_1 and d_2 are large. We find that it also occurs for small d_1 and d_2 when R_b is small.

A new type of stereogram was devised for this study, in which the same periodic image is presented to both eyes (Fig. 2B), and depth results from the "wallpaper" effect. Each "wallpaper stereogram" contains many dot pairs of the type shown in Fig. 1 arranged in a regular array. All pairs have the same disparity, d_b, and orientation, Θ_b. In addition, all pairs within a row have the same separation, R_b. However, R_b is increased from row to row as one moves up the stereogram. Thus the disparity gradient, d_b/R_b, changes systematically over the stereogram.

For an initial experiment, separate stereograms were constructed for each of four angles, Θ_b, and four disparities, d_b. A range of R_b was chosen for each stereogram so that fusion was obtained near the top and diplopia near the bottom. Stereograms were drawn on a hard-copy unit (Tektronix 4631) and measured 15 by 20 cm each.

Three subjects viewed the stereograms from 50 cm and reported the number of the row that appeared to fall at the boundary between regions of fusion and diplopia, the row at which fusion and diplopia seemed equally likely to occur.

In a second experiment, the viewing distance was varied in order to extend the range of disparities studied. A set of 15 stereograms differing in disparity but not in orientation ($\Theta_b = 90$) were viewed from three distances (25, 50, and 100 cm).

Fusion was not always obtained above the reported transition row, and scrutiny of dots often caused diplopia. Diplopia always occurred below the reported transition row.

The dot separation, R_b, was determined for each of the rows reported by subjects in three observations of a stereogram. These were averaged to obtain a single estimate of the critical dot separation, $\hat{R}_b$, which marked the boundary between fusion and diplopia. Transition values for one observer are shown in Fig. 3 as a function of d_b. Separate curves have been drawn in Fig. 3A for each angle Θ_b and in Fig. 3B for each viewing distance.

0036-8075/80/0509-0615$00.50/0